Short-pulse dynamics in strongly nonlinear dissipative granular chains

Alexandre Rosas
Departamento de Física, Universidade Federal da Paraíba, João Pessoa, Caixa Postal 5008–CEP 58.059-970, Paraíba, Brazil

Aldo H. Romero
Libramiento Norponiente 2000, 76230, Fraccionamiento Real de Juriquilla, Cinvestav-Querétaro, Querétaro, Querétaro, Mexico

Vitali F. Nesterenko
Department of Mechanical and Aerospace Engineering, University of California at San Diego, La Jolla, California 92093-0411, USA

Katja Lindenberg
Department of Chemistry and Biochemistry, and Institute for Nonlinear Science, University of California at San Diego, La Jolla, California 92093-0340, USA

(Received 4 August 2008; revised manuscript received 7 October 2008; published 12 November 2008)

We study the energy decay properties of a pulse propagating in a strongly nonlinear granular chain with damping proportional to the relative velocity of the grains. We observe a wave disturbance that at low viscosities consists of two parts exhibiting two entirely different time scales of dissipation. One part is an attenuating solitary wave, dominated by discreteness and nonlinearity effects as in a dissipationless chain, and has the shorter lifetime. The other is a purely dissipative shocklike structure with a much longer lifetime and exists only in the presence of dissipation. The range of viscosities and initial configurations that lead to this complex wave disturbance are explored.

DOI: 10.1103/PhysRevE.78.051303 PACS number(s): 45.70.−n, 46.40.Cd, 43.25.+y, 05.65.+b

I. INTRODUCTION

Granular chains under impulse loading are known to support a rich variety of excitations [1–6]. The precise nature of the excitations depends on a number of features that include the particular granular configurations, state of precompression, dimensionality, shape of initial disturbance and, of particular interest to us in this work, viscosity. Consider first the behavior of a monodisperse one-dimensional chain in which the granules are placed side by side, just touching but without precompression. A velocity v_0 imparted to a single grain quickly evolves into a solitary wave carrying energy whose dynamical evolution depends on the nature of the granules. In particular, for elastic spherical grains one obtains a solitary wave that resides on about 5–7 granules and whose velocity depends on its amplitude [1].

We are interested in the effect of viscosity on the propagation of such an initial excitation. There are a number of different sources and descriptions of viscous effects [7–13], and in [5] we studied the dynamics of a pulse in one such case, when the granular chain is immersed in a viscous medium that gives rise to a Stokes drag proportional to grain velocity. Here we consider the more prevalent situation in which the viscosity arises from the interaction between the grains as one grain rubs against another, expanding on our earlier results for this case [6,14,15]. Here the dissipative contributions are proportional to the relative velocities of grains in elastic contact. It should be noted that in experiments on a chain immersed in some liquids the main dissipative contribution was also found to be proportional to the relative velocities of grains (rather than a Stokes drag term) due to the expulsion of liquid from the area of developing elastic contact [14]. While the former viscous interaction leads to energy and momentum loss to the medium, the latter involves only internal dissipative forces and is consequently momentum conserving. If there were only binary collisions in the chain, the momentum conserving dissipation would be one possible dynamical description of the usual parametrized coefficient of restitution [16].

Our model is the simplest example of a strongly nonlinear discrete system that can be verified experimentally. It consists of a chain of granules that interact via the purely repulsive power-law potential

$$V(\delta_{k,k+1}) = \frac{a}{n}|\delta|_{k,k+1}^{n}, \quad \delta \leqslant 0,$$

$$V(\delta_{k,k+1}) = 0, \quad \delta > 0, \tag{1}$$

where

$$\delta_{k,k+1} \equiv y_k - y_{k+1}. \tag{2}$$

Here a is a prefactor determined by Young's modulus E, the Poisson ratio σ, and the principal radius of curvature R of the surfaces at the point of contact [16,17]; y_k is the displacement of granule k from its equilibrium position. The exponent n depends on the shapes of the contacting surfaces. For spherical granules (Hertz potential) $n=5/2$ and $a=[E/3(1-\sigma^2)]\sqrt{2R}$ [17]. The force between two grains is nonzero only when the grains are in contact, and consists of the mechanical force which is the negative derivative of the potential, and a viscous force that is proportional to the relative velocity of the interacting granules. We introduce the rescaled position x_k, time t, and viscosity coefficient γ used in Refs. [5,6],

$$x_k = \frac{y_k}{b}, \quad t = \frac{v_0 \tau}{b}, \quad \gamma = \tilde{\gamma}\frac{b}{m v_0}, \quad b \equiv \left(\frac{m v_0^2}{a}\right)^{1/n}, \quad (3)$$

where y_k, τ, and $\tilde{\gamma}$ are the corresponding unscaled quantities. The equation of motion for the kth grain then takes the form

$$\ddot{x}_k = [\gamma(\dot{x}_{k+1} - \dot{x}_k) - (x_k - x_{k+1})^{n-1}]\theta(x_k - x_{k+1}) + [\gamma(\dot{x}_{k-1} - \dot{x}_k) + (x_{k-1} - x_k)^{n-1}]\theta(x_{k-1} - x_k), \quad (4)$$

where a dot denotes a derivative with respect to t. The Heaviside function $\theta(y)$ ensures that the elastic and the viscous grain interactions exist only if the grains are in contact. Note that in this scaled equation of motion the constant a as well as the mass have been scaled out, and the initial velocity imparted to a grain is now unity. In the absence of viscosity an initial impulse given to one grain of the chain of otherwise resting grains placed side by side quickly settles into a forward propagating stationary pulse that is increasingly narrow with increasing $n>2$. As we will show, and as one might expect, the viscosity results in an overall exponential energy dissipation. In a viscous medium, if a Stokes drag is the dominant source of dissipation, this is essentially all that the viscosity does [5], so that the pulse simply keeps moving without changing its shape but with a decreasing amplitude (and consequently velocity). Remarkably, in the present situation with dissipation determined by the relative velocity of grains the behavior is entirely different. Below a critical viscosity, there is a steady removal of energy from the pulse, part of which contributes to the formation of a long tail created behind it from which energy is dissipated much more slowly. The removal of energy from the leading pulse is rapid because, being very narrow, it has large velocity gradients, The long tail that evolves behind it loses energy far more slowly because the velocity gradients there are very small [6].

Exact analytic solutions to the equations of motion (4) appear unattainable, and so in this work we rely heavily on numerical simulations, with analytic arguments where possible. In Sec. II we present a detailed study of the propagation of an impulse along a viscous chain when the granules are initially placed side by side with no gaps and no precompression. In Sec. III we explore the effects of an initial precompression on the propagation of the impulse, and briefly comment on the effects of initial gaps. A summary of our findings is presented in Sec. IV.

II. DYNAMICS WITH NO PRECOMPRESSION AND NO GAPS

Consider a granular chain in which the granules are placed side by side, just touching but without precompression. This situation is referred to in Ref. [2] as a "sonic vacuum" because such a system does not support sound waves. In the next section we will relax this condition. A velocity is imparted to a single grain at one end of the chain. Below a critical viscosity, after a short time in which a small amount of energy is lost through some back-scattering of nearby granules in the wake, almost all of the impact energy resides in a forward traveling wave that has an unusual two-part structure which is formed very rapidly and comes about as follows [6]. A pulse similar to a narrow solitary wave caused by the strongly nonlinear forces in the discrete medium is generated. This "primary pulse," being spatially very narrow, exhibits high velocity gradients that lead to a loss of its energy. Some of the lost energy is simply dissipated, but part of the energy of the leading pulse goes into a quasistatic compression that appears behind the primary pulse because the forward displacements of the particles closer to the impacted end are larger than the corresponding displacements of particles further away from this end due to the attenutation of the velocity of the particles in the propagating wave. This compression, and the associated pulse that arises as a result ("secondary pulse"), are entirely dependent on the presence of dissipation. As a result, this two-wave structure is not observed in the usual dissipationless models. The secondary pulse is very broad and is therefore far more persistent than the primary pulse because it has much smaller velocity gradients. A typical progression with time of the velocity profile for a small viscosity is shown in Fig. 1. The figure exhibits all the characteristics discussed above, specifically, the narrow decaying primary pulse and the evolving secondary pulse. A more detailed discussion of this figure will be presented later.

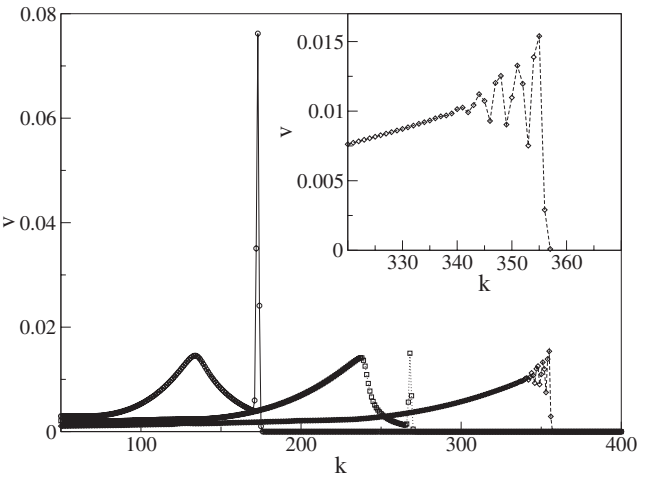

FIG. 1. Time snapshots of the velocity profile for small viscosity (γ=0.02). The progression of the profile is easily recognizable as the composite pulse moves forward, the secondary pulse steepens, generating oscillatory behavior, and the primary pulse disappears. The times are 500, 900, and 1400 and n=5/2. Inset, detailed view of the crest of the velocity profile at time 1400.

The total energy of the system as a function of time is shown in the inset in Fig. 2 for two values of n and three values of γ. In our scaled units, the initial energy is 1/2. The attenuation of the energy of the "primary" and "secondary" portions for the case n=5/2 and γ=0.01 is shown in Fig. 2, demonstrating the separation of time scales for energy dissipation. The primary pulse is a highly nonstationary portion of the wave that exhibits a steep exponential decay of the energy. The energy dissipation slows down drastically as the primary pulse vanishes and only the more persistent secondary pulse remains. Dissipation of energy in the rapid decay regime is faster for higher n. This behavior is due to the larger velocity gradients in the primary pulse whose width decreases with increasing n [2].

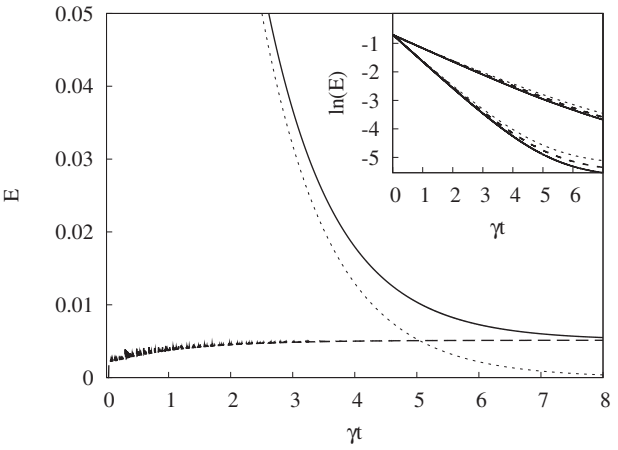

FIG. 2. Breakdown of the total energy (solid line) into portions associated with the primary pulse (dotted line) and the secondary pulse (dashed line) for $n=5/2$ and $\gamma=0.01$. Inset, time evolution of the total energy, where two sets of three curves are shown, corresponding to $n=2.2$ (upper set) and 2.5 (lower set) in the Hertz potential. Each set shows results for $\gamma=0.01$ (dotted line), 0.005 (dashed line), and 0.001 (solid line). The early rapid decay mainly reflects the rapid energy loss of the primary pulse. The remaining energy stored in the secondary pulse eventually dissipates on a much longer time scale.

To set the stage for further discussion, we recall the successful treatment of this problem in the absence of dissipation based on a long-wavelength approximation [1–3,5]. This analysis, based on a continuum description, is extremely successful despite the fact that the pulse is very narrow in the underlying discrete system, i.e., in spite of the fact that a continuum approximation assumes that the particle characteristic length is much smaller than the wavelength, which in fact it is not. For large n, when the pulse is extremely narrow, a decidedly discrete binary collision approximation works even better [18], but the continuum approximation still works well at least qualitatively. Some of the effects of discreteness are captured by expanding $x_{k\pm1}$ about x_k in a Taylor series up to fourth order (the usual second order expansion would of course not capture any such effects). The continuum equation is obtained by neglecting the one-sidedness of the potential, that is, ignoring the fact that there are no attractive forces in the problem. This works because the solution is assumed to apply only to the compressed portion of the chain, and to be identically equal to zero outside of this region. The equation of motion for $n>2$ obtained in this way is [2]

$$\frac{\partial^2 x}{\partial t^2} = \frac{\partial}{\partial k}\left[-\left(-\frac{\partial x}{\partial k}\right)^{n-1} + \frac{n-1}{24}\left(-\frac{\partial x}{\partial k}\right)^{n-2}\frac{\partial^3 x}{\partial k^3}\right] - \frac{1}{24}\frac{\partial^3}{\partial k^3}\left[\left(-\frac{\partial x}{\partial k}\right)^{n-1}\right]. \tag{5}$$

This equation admits a solution of the form [2],

$$\left(-\frac{\partial x}{\partial \xi}\right) = A_0 \sin^m \alpha\xi, \tag{6}$$

where $\xi=k-c_0t$, c_0 is the pulse velocity, and

$$m = \frac{2}{(n-2)}, \quad \alpha = \left(\frac{6(n-2)^2}{n(n-1)}\right)^{1/2}, \quad c_0 = \left(\frac{2}{n}\right)^{1/2} A_0^{(n-2)/2}. \tag{7}$$

A solitary wave is constructed by retaining this solution over one period, $0\leq\alpha(k-c_0t)\leq\pi$, and setting $\partial x/\partial\xi$ equal to zero outside of this range. This solution does not satisfy the velocity pulse initial condition because it is meant to describe the system after a short initial transient whereupon it settles into this traveling configuration. One can go further and take advantage of the fact that almost all of the initial energy resides in this pulse (an extremely small portion is lost to back-scattering [3,5]). Using conservation of energy arguments and dealing carefully with the fact that due to nonlinearity the kinetic (K) and potential (U) energies are not equal but instead obey a generalized equipartition theorem [19], one further finds that $K/U=n/2$ so that $K=n/[2(n+2)]$. The kinetic energy can be calculated directly by explicit integration,

$$K = \int_0^{\pi/2\alpha} \dot{x}(\xi)d\xi = \frac{c_0^2 A_0^2}{2\alpha} I\left(\frac{4}{n-2}\right), \tag{8}$$

where

$$I(s) = \int_0^{\pi} \sin^s \theta d\theta = 2^s \frac{\Gamma^2\left(\frac{s+1}{2}\right)}{\Gamma(s+1)}. \tag{9}$$

This result together with the generalized equipartition theorem then leads to explicit values for c_0 and A_0. In particular, for spherical granules we find $c_0=0.836$ and $A_0=0.765$ [5].

In the presence of dissipation, a similar expansion of the equations of motion (4) leads to an additional contribution in the continuum problem,

$$\frac{\partial^2 x}{\partial t^2} - \gamma\frac{\partial^2}{\partial k^2}\left(\frac{\partial x}{\partial t}\right) = \frac{\partial}{\partial k}\left[-\left(-\frac{\partial x}{\partial k}\right)^{n-1} + \frac{n-1}{24}\left(-\frac{\partial x}{\partial k}\right)^{n-2}\frac{\partial^3 x}{\partial k^3}\right] - \frac{1}{24}\frac{\partial^3}{\partial k^3}\left[\left(-\frac{\partial x}{\partial k}\right)^{n-1}\right]. \tag{10}$$

Unfortunately, we have not found an exact solution to this equation, especially one that at low viscosities captures the two contributions to the solution whose features we have described on the basis of numerical simulations. In the following two sections we discuss the dynamics of this solution mainly on the basis of simulations. At low viscosities, this discussion is reasonably organized into a separate discussion for each of the two portions of the excitation, the primary and the secondary pulses, because their evolution and decay involves such disparate time scales. However, we wish to stress that in spite of this separation, the pulse is one entity that consists of two interdependent parts rather than a superposition of two independent entities. Furthermore, clearly identifiable primary and secondary pulses occur only if the viscosity is sufficiently small. This point, as well as the behavior at higher viscosities, will be described in more detail below.

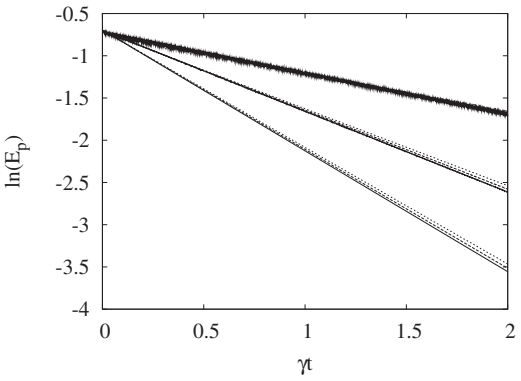

FIG. 3. The primary pulse energy decays exponentially, as $e^{-2u\gamma t}$, with time. From top to bottom, the three groups of lines correspond to $n=3$, 5/2, and 2.2. For each n, there are three values of γ, 0.01 (dotted line), 0.005 (dashed line), and 0.001 (solid line). The slopes of the curves change slightly with γ but are equal within a 10% margin ($u=0.20\pm0.02$ for $n=2.2$, $u=0.46\pm0.02$, for $n=5/2$, and $u=0.70\pm0.03$ for $n=3$).

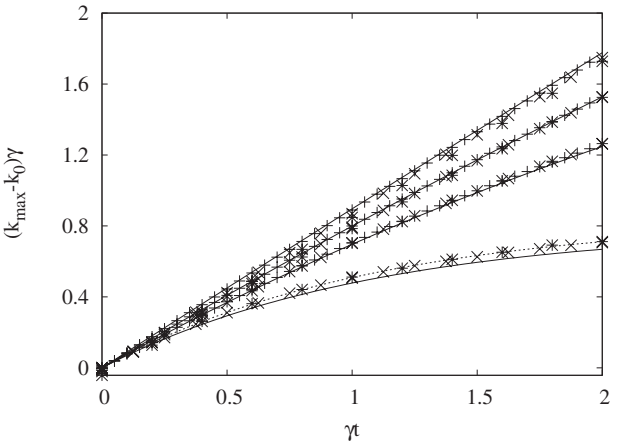

FIG. 4. Position of the grain with maximum velocity as a function of time for the same values of n (upper three groups) and γ (0.001 plus signs, 0.005 crosses, and 0.01 stars) as in Fig. 3. The lowest group of curves is for $n=7$. Here, $k_0=\frac{\pi}{2\alpha}$. The solid lines are the theoretical predictions according to Eq. (16). The dotted curve for $n=7$ is obtained from the binary collision approximation.

A. Primary pulse

As in the dissipationless case, the primary pulse forms quickly following the initial velocity impact due to the strong nonlinearity and dispersion. The pulse travels along the chain with diminishing speed (and with an evolving tail) since its amplitude decreases due to dissipation. As noted above and as is apparent in Fig. 2, the loss of energy due to dissipation is initially essentially exponential as long as the energy is mainly stored in the primary pulse. While we know that it cannot be the entire solution because it does not account for the secondary pulse, we assume a solution of the form Eq. (6) but with a time-dependent amplitude and velocity. This captures the behavior of the primary pulse if it retains its shape as it loses energy, and is at best expected to hold as long as there is a prominent primary pulse, that is, for times $\gamma t \lesssim 1$,

$$\left(-\frac{\partial x}{\partial \xi}\right) = A(t)\sin^{2/(n-2)}\alpha\xi(k,t), \tag{11}$$

where

$$\xi(k,t) = k - \int_0^t c(t)dt \tag{12}$$

and

$$c(t) = \sqrt{\frac{2}{n}}A^{(n-2)/2}(t). \tag{13}$$

We may speculate that this approach is valid as long as the strong nonlinearity and dispersion are more or less balanced as in a nondissipative chain, which is the case for the primary pulse. To choose a specific functional form for $A(t)$ we must rely on the simulation results and observe that to times of order $\gamma t \sim 1$ the decay of the energy, as exhibited in Fig. 2, is exponential. This is confirmed in more detail in Fig. 3, where it is evident that for all the values of n and γ in the figure the decay is well described by an exponential. Furthermore, the slope is fairly insensitive to the value of γ, so at least to a first approximation the energy decays as $e^{-2u\gamma t}$ where u is a constant (and the 2 is introduced for convenience). While the notation E in Fig. 2 indicates the total energy and the notation E_P in Fig. 3 indicates the primary pulse energy, at the early times of Fig. 3 they are essentially the same. The decay of the amplitude and the pulse velocity with the assumed form Eq. (11) then are

$$A(t) = A_0 e^{-2u\gamma t/n}, \quad c(t) = c_0 e^{-(n-2)u\gamma t/n}, \tag{14}$$

and therefore

$$\xi(k,t) = k - c_0\frac{n}{u\gamma(n-2)}(1-e^{-(n-2)u\gamma t/n}). \tag{15}$$

The validity of the assumed form for the primary pulse can be tested numerically in a number of ways. For instance, our trial solution predicts that the position of the maximum of the pulse should be [5]

$$k_{\max} = \frac{\pi}{2\alpha} + \frac{c_0}{\gamma u}\frac{n}{(n-2)}(1-e^{-nu\gamma t/(n-2)}). \tag{16}$$

In Fig. 4 we compare this prediction with the numerical results. According to Eq. (16), the curves corresponding to different values of γ should collapse for each n, and indeed we have a clear collapse. Moreover, using the values of u obtained from the energy decay, we observe excellent agreement. As a test of the continuum approximation concept, we have included results for the very high value $n=7$. Here we observe a deviation between the numerical results (symbols) and the solid curve obtained from Eq. (16) with u determined from the energy decay curve and c_0 obtained via the continuum approximation. For this large value of n the pulse is extremely narrow, and so we tested an alternative binary collision approximation in which we assume that only two granules are involved in a collision at any one time [18]. With c_0 calculated from this approximation we obtain the dotted line, which is in excellent agreement with the simulations. We stress that in any case the curve collapse predicted by the

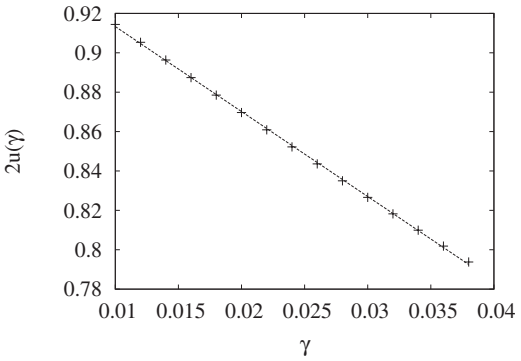

FIG. 5. Energy decay exponent. The symbols represent the results of the fitting of the primary pulse exponential energy decay and the line $2u(\gamma)=0.956\,464-4.314\,51\gamma$, which is the best linear fit of those points.

form (16) is observed for all the values of n and γ exhibited in the figure. This confirms that the pulse position is indeed an exponential function of γt.

While Fig. 3 shows an exponential decay of the energy of the primary pulse with time, there is a small spread in the slope of the logarithm E_P vs γt, indicative of a mild γ dependence of u on γ. We thus write more accurately

$$E_P \sim e^{-2u(\gamma)\gamma t}. \tag{17}$$

The dependence of u on γ, which is essentially linear and indeed mild, is seen in Fig. 5. We also confirm our ubiquitous assumption that the total energy and the energy in the primary pulse are essentially equal up to times of order $\gamma t \sim 1$. This is shown in Fig. 6, where we plot the total energy (on a logarithmic scale) vs $2u(\gamma)\gamma t$. The deviations from this behavior that set in beyond these times are greater for larger viscosities.

B. Secondary pulse

Returning to Fig. 1, we follow the continuing history of the excitation. Above we have described the behavior of the primary pulse during the course of its existence. The figure illustrates the evolution of a long-lived secondary pulse during this time interval. This secondary pulse, also being a nonlinear disturbance, continues to change in shape. The pulse steepens (becoming more and more asymmetric) as its peak travels faster than the bottom right of the peak. Note that the primary and secondary pulses have comparable amplitudes even while they are still distinguishable before the primary pulse dissipates. When the secondary pulse is sufficiently steep, dispersion begins to prevail and the front displays oscillatory structure with peaks that are a few grains wide. This is shown in the inset of Fig. 1. The secondary pulse is shocklike, with velocities of the grains in the pulse at least an order of magnitude smaller than the pulse phase speed.

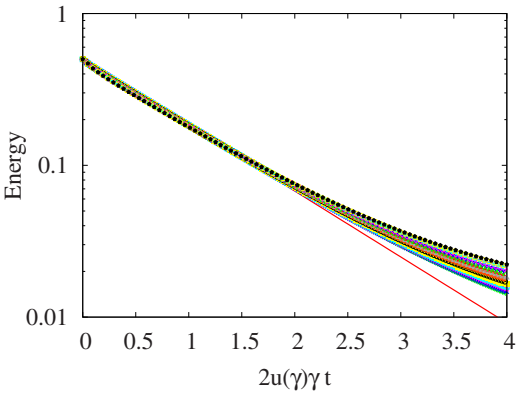

FIG. 6. (Color online) Early total energy decay for $n=5/2$. The line is the expected behavior according to our hypothesis $E=(1/2)\exp[-2u(\gamma)\gamma t]$, while the different symbols represent the energy decay for different values of γ ranging from 0.01 (lowest curve) to 0.039 (highest curve).

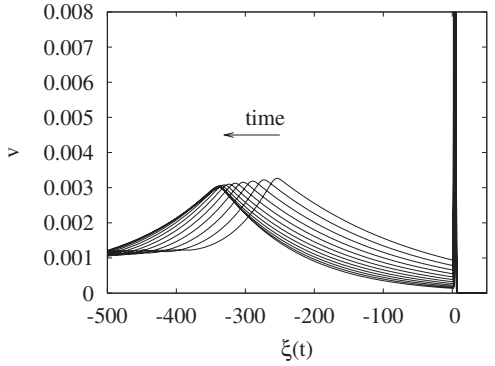

FIG. 7. Snapshots of the velocities of the grains at early times ranging from 40 to 95 in steps of 5 in nondimensional units ($n=5/2$ and $\gamma=0.005$). The abscissa is the moving variable $\xi(t)\equiv k-\int_0^t c(t)dt$, where $c(t)$ is the time-dependent velocity of the primary pulse, and k denotes the granule in the chain. Eventually the primary pulse and the compression behind it vanish and the secondary pulse continues to move at an essentially constant velocity.

Figures 7 and 8 detail the behavior of the secondary pulse while the primary pulse has not yet disappeared. At first the secondary pulse moves more slowly than the primary, but this trend reverses as the primary pulse slows down with its loss of energy and the peak of the secondary pulse acquires

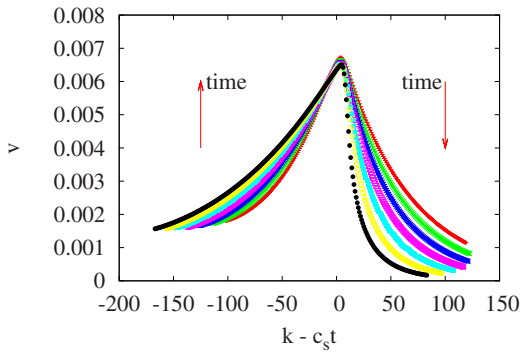

FIG. 8. (Color online) Snapshots of the velocity profiles of the secondary pulse for $n=5/2$ and $\gamma=0.01$ at different times, with increase upward on the left-hand side of the pulse and downward on the right-hand side, consistent with the steepening of the pulse with time. The abscissa is now the moving variable with respect to the essentially constant velocity of the peak of the secondary pulse.

an essentially constant velocity. Both figures show that the secondary pulse is asymmetric, generating an extremely persistent tail of essentially equal velocity granules behind it (not shown explicitly in the figures). This asymmetry sharpens with time, as is made evident in Fig. 1.

The velocity of the peak of the secondary pulse is constant throughout this early portion of its history, as seen clearly in Fig. 8, where the abscissa for all the times shown is scaled with the same velocity c_s. It is furthermore extremely interesting that this peak velocity can be associated with a "speed of sound" in the following sense (even though this system in the initial uncompressed state is a sonic vacuum [1,2]). That is, if k denotes the position of the grain with maximum velocity, we observe that the velocities of grains k and $k+1$ are related as

$$v_k(t) = v_{k+1}\left(t + \frac{1}{c_s}\right) \approx v_{k+1}(t) + \dot{v}_{k+1}(t)\frac{1}{c_s}, \tag{18}$$

where the speed c_s is expressed in units of grains per unit time, and the approximation follows from a Taylor series expansion to first order. Therefore, the relative velocity $v_k^{(R)} = v_k - v_{k+1}$ can be written as

$$v_k^{(R)} = \dot{v}_{k+1}\frac{1}{c_s}. \tag{19}$$

Further, we can thus write

$$c_s(v_k^{(R)} - v_{k-1}^{(R)}) = \dot{v}_{k+1} - \dot{v}_k. \tag{20}$$

Since the medium is precompressed (because of the first pulse), we may linearize Eq. (4) [2]

$$\dot{v}_k = -\Delta^{n-1} + \left(\Delta + v_{k-1}^{(R)}\frac{1}{c_s}\right)^{n-1} \simeq \Delta^{n-2}(n-1)\frac{v_{k-1}^{(R)}}{c_s}, \tag{21}$$

$$\dot{v}_{k+1} = -\left(\Delta - v_k^{(R)}\frac{1}{c_s}\right)^{n-1} + \Delta^{n-1} \simeq \Delta^{n-2}(n-1)\frac{v_k^{(R)}}{c_s}, \tag{22}$$

where $\Delta \equiv x_k - x_{k+1}$ is the compression. Hence,

$$c_s(v_k^{(R)} - v_{k-1}^{(R)}) = (n-1)\frac{\Delta^{n-2}}{c_s}(v_k^{(R)} - v_{k-1}^{(R)}), \tag{23}$$

so that the sound speed is finally given by (see Eq. (1.114) in [2])

$$c_s = \sqrt{(n-1)\Delta^{n-2}}. \tag{24}$$

We can compare the speed of sound based on Eq. (24) using Δ obtained from numerical simulations, and the speed of the secondary pulse maximum, also obtained directly from numerical simulations. Figure 9 shows the agreement between the two to be excellent, as do the representative values in Table I. The figure and the table exhibit this agreement via the dependence of these two speeds on γ, which is the parameter that determines the precompression Δ behind the primary pulse. The variation of the speeds with γ obtained from the numerical results by a best fit goes as $\gamma^{0.24}$. The dramatic agreement observed in the figure is also found for other values of n, as illustrated in Table I. As γ increases, the time it takes for the second pulse to "catch" the first one decreases and it becomes difficult to obtain the sound speed. Therefore, we are only able to exhibit this speed for small viscosities.

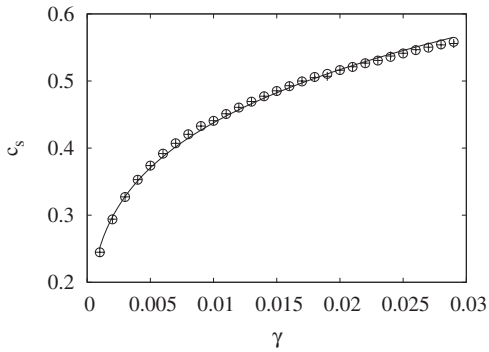

FIG. 9. The plus signs show the sound speed for different values of γ in the precompressed region behind the primary pulse as found from Eq. (24) and numerical simulation results for the precompression Δ when $n=5/2$. The circles show the maximum of the secondary pulse for $n=5/2$, also obtained directly from numerical simulations. The line represents a power-law best fit to the data (the difference between fitting the circles and the plus signs is negligible).

Consider next the energy in the secondary pulse. The increase in this energy is observed to be of the form $B(1-e^{-2u\gamma t})$, where B depends on n and γ and is the maximum energy of the secondary pulse. More accurately,

$$E_S(t) = B(\gamma)(1 - e^{-2u(\gamma)\gamma t}). \tag{25}$$

In Fig. 10 we plot $B(\gamma)$ as a function of γ for $n=5/2$, showing a fairly linear dependence. However, although the trend is captured when we plot $E_S(t)/B(\gamma)$ vs $2u(\gamma)\gamma t$ as in Fig. 11, we do not observe a clean collapse as predicted by Eq. (25), indicative of a more complex γ dependence. In any case, the secondary pulse reaches its maximum value over a time scale of order $\gamma t \sim 1$ and then remains essentially constant over a much longer time scale, although eventually its energy will also be dissipated.

C. Higher viscosities

The detailed results presented to this point are associated with small values of γ. In this regime it has been reasonable to speak of two pulses as though they were separate entities,

TABLE I. Comparison of secondary peak pulse velocity and c_s calculated from the precompression for two values of the potential exponent n and various values of the dissipation parameter.

$n=2.2$			$n=2.5$		
γ	Pulse vel.	c_s	γ	Pulse vel.	c_s
0.001	0.56	0.55	0.001	0.25	0.25
0.005	0.66	0.66	0.005	0.38	0.38
0.01	0.71	0.71	0.01	0.44	0.44

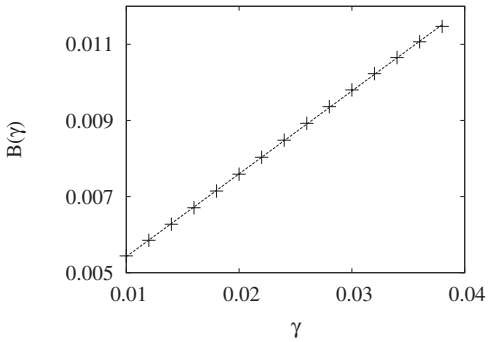

FIG. 10. Secondary pulse energy saturation constant for $n=5/2$. The symbols represent the results of fitting Eq. (25), and the line $B(\gamma)=0.003\,246\,36+0.217\,601\gamma$ is the best linear fit for these points.

the primary being mainly due to nonlinearity and discreteness, and the secondary caused mainly by dissipation and nonlinearity. Nevertheless, it is not inappropriate for these low viscosities to speak of a "separation" of pulses. The primary pulse causes the precompression that underlies the secondary pulse, and in this sense both together are a single entity. Summarizing this regime, for small viscosities ($\gamma\leqslant 0.03$) the secondary pulse reaches a critical slope for transition to an oscillatory profile before catching the primary pulse, while the primary pulse loses almost all of its energy before being absorbed by the secondary pulse (Fig. 1; the oscillatory shock profile first emerges when the secondary pulse is in the vicinity of particle 300, not shown in the figure). Note that a critical viscosity for a transition from an oscillatory to a monotonous profile of a shock wave is found in [15]. We have observed that in this small-γ regime the maximum velocity in the secondary pulse increases with increasing viscosity because larger dissipation is associated with a greater compression, resulting in a secondary pulse of higher amplitude. For very small γ ($\lesssim 0.002$) the secondary pulse has an almost imperceptible amplitude on our numerical scale (and of course it disappears entirely when $\gamma=0$), and the primary pulse has a very long life. However we do not find a transition to a regime without a secondary pulse for any finite value of γ. The secondary pulse fades away smoothly with diminishing γ.

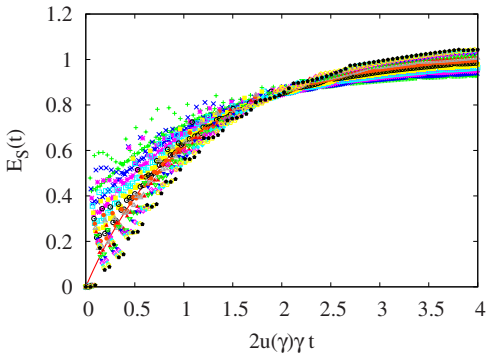

FIG. 11. (Color online) Collapse of the energy behind the primary pulse for $n=5/2$ and different values of γ. The line is $1-e^{-2u(\gamma)\gamma t}$, the behavior according to the hypothesis equation (25), while the symbols represent the simulation results.

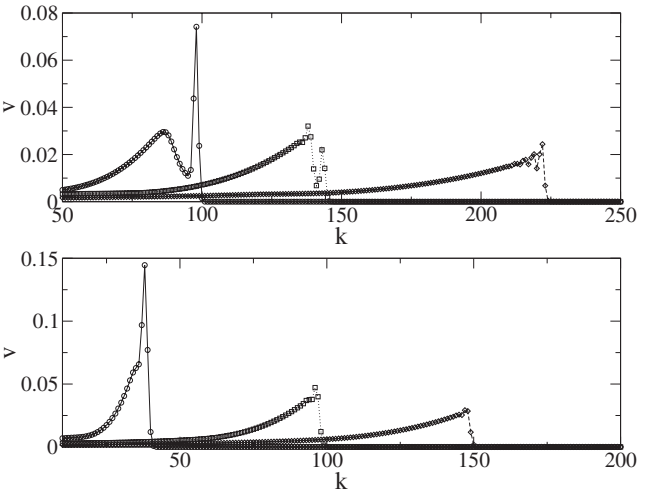

FIG. 12. Upper panel: Snapshots of the velocity profile for intermediate viscosity ($\gamma=0.04$, $n=5/2$) at different times, 140, 220, and 400. Lower panel: Snapshots of the velocity profile for large viscosity ($\gamma=0.1$, $n=5/2$) at different times, 100, 300, and 500.

For intermediate viscosities ($0.04\leqslant\gamma\leqslant 0.07$) the secondary pulse catches up with the primary pulse while the primary pulse still has an amplitude comparable to the secondary (upper panel of Fig. 12). As in the previous case, after the first pulse disappears, the secondary pulse propagates as a shocklike wave with an oscillatory front caused by the dispersion.

For large viscosities ($\gamma\geqslant 0.07$) there is no clear distinction between the primary and secondary pulses. Actually, for viscosities $\gamma\geqslant 0.1$ it is no longer appropriate to think of two separate pulses (lower panel of Fig. 12). From almost the beginning, there is a single shocklike structure of dissipative origin with a sharp monotonic front. Nevertheless, it should be noted that the first pulse is always evident, albeit for a very short time. In Fig. 13 we see that it takes about four granules for it to develop fully, and that the dynamics up to 10 grains or so is always the same, that is, the shape of the pulse and the time it takes to develop are essentially the same for viscosities ranging from 0 to 0.1. After this early time either the second pulse appears behind the first pulse (small γ), or the first pulse appears to be essentially deformed into the second pulse (larger γ).

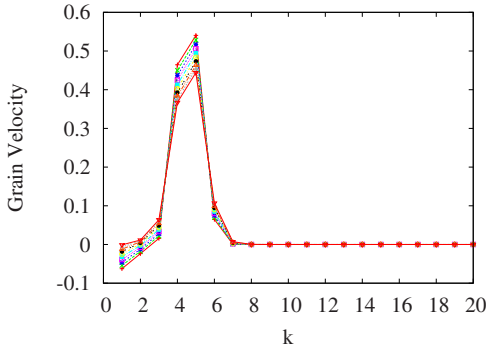

FIG. 13. (Color online) Early dynamics. The first pulse always occurs at early times. At the beginning, the only role of the viscosity is to dissipate energy. The shape of the pulse and the time it takes to develop it is the same for γ ranging from 0.01 to 0.1

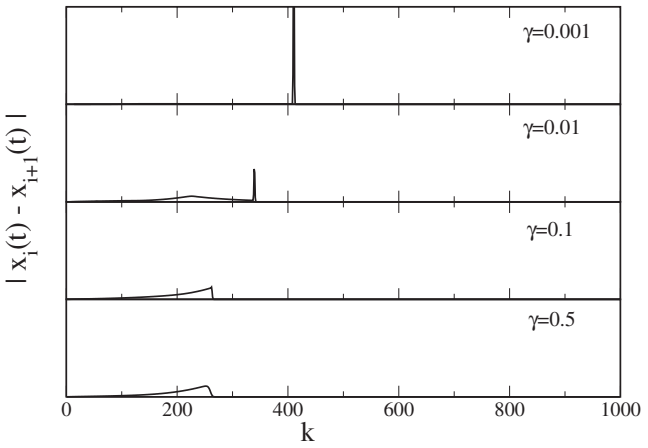

FIG. 14. Grain compression along the chain with no precompression at 50 000 iterations. Panel progression shows the chain at the same instant of time under the effect of increasing dissipation.

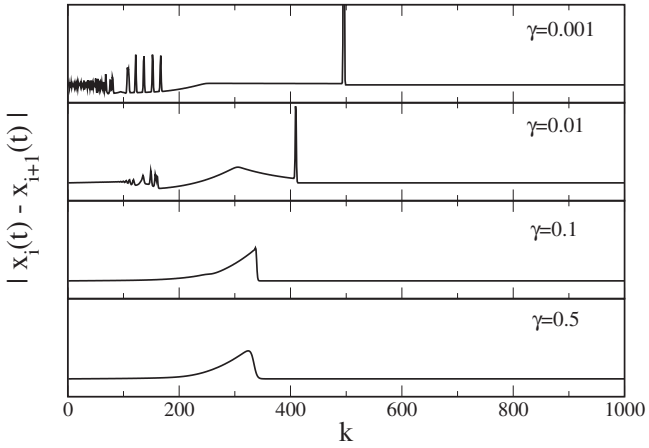

FIG. 15. Pulse propagation in a precompressed chain in which the precompression is 100 times weaker than the dynamic displacement imparted by the initial pulse. Viscosity increases downward, as indicated. The scale on the *y* axis in the first and second panels goes from −0.01 to 0.1, in the third panel from 0.0 to 0.4, and in the fourth panel from 0.4 to 0.8.

III. DYNAMICS WITH PRECOMPRESSION AND WITH INITIAL GAPS

The results presented up to this point deal with a chain in which the granules are initially placed side by side, with no precompression and with no gaps (i.e., a sonic vacuum [1,2]). In this section we explore the consequences of relaxing these assumptions. In particular, we explore the way in which a variation in the initial placement of granules modifies or otherwise distorts the two-component wave disturbance discussed above. Based on numerical simulations, we present these effects through a series of figures.

The first of these figures, Fig. 14, is simply a recap of previous results that facilitates our discussion. In this figure there is no precompression, and we show the grain compression wave structure at a particular instant of time after 50 000 iterations as the damping increases. At extremely low damping there is a solitary wave accompanied by an extremely low amplitude secondary wave that is not visible on the scale of the figure. As the viscosity increases, the secondary pulse behind the primary pulse becomes more prominent. Increasing the viscosity further leads to a single shock-type pulse (the primary pulse has already disappeared), with a wider shock front at the larger viscosity.

Next we explore the consequences of precompression, which qualitatively changes our system from a sonic vacuum to a more traditional discrete system with finite sound speed. We ensure mechanical equilibrium by applying appropriate static forces to the end particles of the chain. The next three figures show progressions of increasing viscosity at a given precompression. Viscosity increases from one figure to the next (note the different *y*-axis scales in the three figures). Figure 15 shows the changes introduced by a very small precompression. The features illustrated in Fig. 14 are repeated in this figure at the same instant of time, specifically the presence of a primary and a secondary pulse when the viscosity is small, and, at higher viscosities the single shock-type pulse of increasing front width as viscosity increases. The new feature here, namely, the rarefaction wave and the tail of attenuating compression peaks propagating in the locally unloaded system with zero strain that follow the secondary wave, are due to the precompression. They occur at zero viscosity and survive the effects of low viscosities. The attenuating compression peaks propagating in the locally unloaded system with zero strain are related to the rattling of particles at the impacted end accompanied by the opening and closing of gaps. In Figs. 16 and 17 we see that increasing precompression causes the secondary wave (when it is visible at all) to decrease in amplitude and width, but that the other features (primary wave with trailing rarefaction wave and attenuating oscillatory tail at lower viscosities, single shock-type pulse at higher viscosities) continue to persist. Note that greater precompression leads to a stronger (and therefore faster) primary pulse, an effect that has nothing to do with the viscosity but that we just point out for completeness of the description.

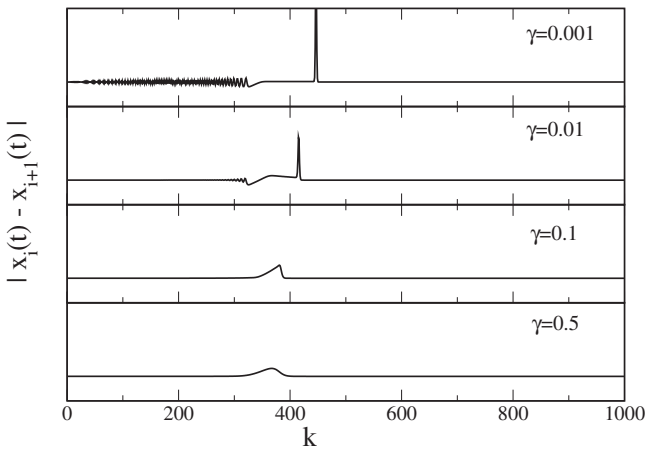

FIG. 16. Pulse propagation in a precompressed chain in which the precompression is 10 times weaker than the dynamic displacement imparted by the initial pulse. Viscosity increases downward, as indicated. The scale on the *y* axis in the first and second panels goes from −0.01 to 0.1, in the third panel from 0.0 to 0.4, and in the fourth panel from 0.4 to 0.8.

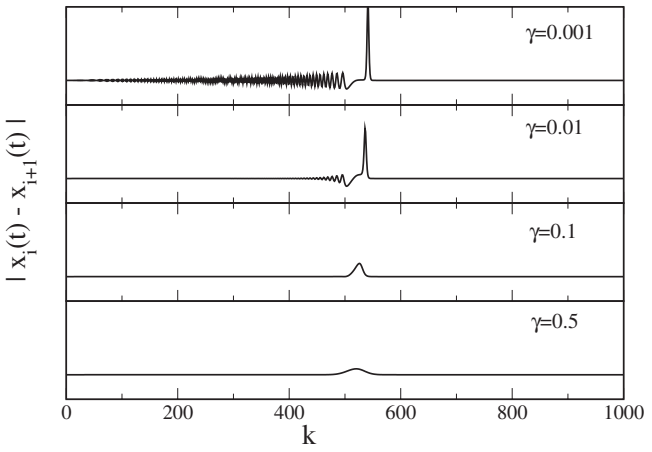

FIG. 17. Pulse propagation in a precompressed chain in which the precompression is one-half as large as the dynamic displacement imparted by the initial pulse. Viscosity increases downward, as indicated. The scale on the *y* axis in the first and second panels goes from −0.01 to 0.1, in the third panel from 0.0 to 0.4, and in the fourth panel from 0.4 to 0.8.

Finally, we recall that with weak or zero precompression the velocity of the primary excitation is related to its amplitude in a nonlinear fashion determined by the nonlinearity of the medium (and of course by the dissipation that causes a decrease in the amplitude with time) and essentially unrelated to any speed of sound in the medium. On the other hand, the secondary pulse velocity is related to the compression of the medium that follows the primary pulse and is determined by the speed of sound. With increasing precompression, the speed of sound increasingly determines the speed of disturbance propagation, as we can see, for example, in Fig. 17, where all four panels show essentially the same speed. The larger the precompression, the smaller the effect of the nonlinearity; at sufficiently high precompression relative to the compression caused by the initial pulse, the medium effectively becomes linear.

The introduction of relatively large gaps in the initial distribution of granules causes the system to no longer behave as a collective entity and it will instead resemble a granular gas. We have determined that gaps up to size of order 10^{-5} in our dimensionless units lead to behavior similar to that of the original system. However, beyond this the loss of energy and the character of the excitation begin to change drastically.

IV. SUMMARY

In this work we have explored the interplay of nonlinearity, discreteness, and dissipation in a one-dimensional dense granular chain. In particular, we have expanded on our earlier demonstration of an interesting two-wave structure observed in a dissipative granular chain excited by a δ-force applied to a single grain [6]. One might expect a one-wave structure such as an attenuating solitary wave or an attenuating shock wave—the observation of a complex two-wave structure is certainly unusual. This structure, which occurs at low viscosities (but requires nonzero viscosity), consists of a primary wave characteristic of a discrete nonlinear nondissipative sonic vacuum, and a secondary shocklike long wave due entirely to intergrain contact viscosity. The high velocity gradients in the narrow primary pulse lead to its relatively rapid attenuation, which we have shown numerically to be exponential. We have furthermore shown that the decay rate is essentially proportional to the viscosity γ, with small correction terms of $O(\gamma^2)$. During its lifetime, the speed of the primary pulse is related to its amplitude in the same way as in a nondissipative chain [1–3,5], but now they both decrease with time as the primary pulse dissipates. Some of the dissipated energy is simply lost, while some of the initial energy of the primary pulse is transferred to the secondary pulse caused by the compression left behind by the primary pulse (which would not occur in the absence of viscosity). The much smaller velocity gradients in the secondary pulse cause it to be very long-lived, and its speed is essentially the local speed of sound. Below a critical viscosity the secondary pulse develops a dispersion-induced oscillatory front. There are thus three distinct time scales in this problem: An extremely short scale for the formation of the primary pulse, a relatively rapid time scale of attentuation of the primary pulse, and a very slow time scale for the eventual attenuation of the secondary pulse. At higher viscosities it becomes less and less appropriate to think of the primary and secondary pulses as separate entities. Instead, one observes a spatially lengthening excitation that presents a monotonic front. This description is appropriate after a very short time during which there is always a primary pulse, with formation and evolution characteristics essentially independent of the viscosity. But this primary pulse is dissipated very quickly at higher viscosities and most of the dynamical regime is dominated by the shocklike wave. We have provided a particularly detailed picture of the formation and evolution of the structure when the grains are initially in contact with one another but without precompression (sonic vacuum).

We also explored the consequences of relaxing the initial configuration, particularly to the case of initial precompression. We found that as long as the precompression is small compared to the dynamical compression produced by the initial velocity impulse, the features described above are still observed, albeit somewhat complicated by the appearance of a rarefaction wave and a tail of attentuating compression peaks propagating in the locally unloaded system with zero strain behind the secondary wave. As before, there are distinct primary and secondary waves when the viscosity is low, and (except for very short times) a single shock-type pulse when the viscosity is high. We also observed that increasing precompression leads to increasingly linear behavior in which any oscillatory features decrease in amplitude, and the excitation propagates at essentially the speed of sound in the medium.

Finally, we briefly explored the opposite relaxation of the initial condition, namely, the effect of initial gaps between the grains. When these gaps are extremely small, of size 10^{-5} or smaller in our dimensionless units, the behavior is similar to that of the chain without gaps, but beyond this the character of the dynamics of the excitation changes drastically. We have not explored this regime in detail.

We expect the two-wave phenomenon involving vastly different length and time scales to occur in other nonlinear discrete dissipative systems under conditions of short pulse loading. Examples might include femtosecond-laser generated pulses, waves generated in atomic lattices by bombardment of low density beams of ions, and waves in three-dimensional packings of spherical beads immersed in liquid under short-duration plane explosive loading. While our analysis has focused on one-dimensional chains, we expect the phenomenon to occur in systems of higher dimensions as well, where issues of geometry of the constituents and of the initial loading introduce additional interesting variables. Work along these various directions is in progress.

ACKNOWLEDGMENTS

Acknowledgment is made to the Donors of the American Chemical Society Petroleum Research Fund for partial support of this research (K.L.). This work was supported in part by the Conselho Nacional de Desenvolvimiento Científico e Tecnológico (CNPq) (A.R.), CONACyT Mexico Contracts No. J-59853-F and No. 48783-F (A.H.R.), and NSF Grant No. DCMS03013220 (V.F.N.).

[1] V. F. Nesterenko, Prikl. Mekh. Tekh. Fiz. **24**, 136 (1983) [J. Appl. Mech. Tech. Phys. **24**, 733 (1984)].
[2] V. F. Nesterenko, *Dynamics of Heterogeneous Materials* (Springer, New York, 2001).
[3] E. J. Hinch and S. Saint-Jean, Proc. R. Soc. London, Ser. A **455**, 3201 (1999).
[4] S. Sen, J. Hong, J. Bang, E. Avalos, and R. Doney, Phys. Rep. **462**, 21 (2008), and references therein.
[5] A. Rosas and K. Lindenberg, Phys. Rev. E **68**, 041304 (2003).
[6] A. Rosas, A. H. Romero, V. F. Nesterenko, and K. Lindenberg, Phys. Rev. Lett. **98**, 164301 (2007).
[7] G. E. Duvall, R. Manvi, and S. C. Lowell, J. Appl. Phys. **40**, 3771 (1969).
[8] C. Brunhuber, F. G. Mertens, and Y. Gaididei, Phys. Rev. E **73**, 016614 (2006).
[9] E. Arevalo, Y. Gaididei, and F. G. Mertens, Eur. Phys. J. B **27**, 63 (2002).
[10] N. V. Brilliantov, F. Spahn, J. M. Hertzsch, and T. Pöschel, Phys. Rev. E **53**, 5382 (1996); R. Ramirez, T. Pöschel, N. V. Brilliantov, and T. Schwager, *ibid.* **60**, 4465 (1999); T. Pöschel and N. V. Brilliantov, in *Granular Gases*, Vol. 564 of Lecture Notes in Physics, edited by S. Luding (Springer, Berlin, 2000), pp. 203–212.
[11] M. Manciu, S. Sen, and A. J. Hurd, Physica D **157**, 226 (2001); S. Sen *et al.*, in *AIP Conference Proceedings: Modern Challenges in Statistical Mechanics*, Vol. 658, edited by V. M. Kenkre and K. Lindenberg (AIP, New York, 2003), pp. 357–379.
[12] S. McNamara and E. Falcon, Phys. Rev. E **71**, 031302 (2005).
[13] A. Rosas, J. Buceta, and K. Lindenberg, Phys. Rev. E **68**, 021303 (2003).
[14] E. B. Herbold, V. F. Nesterenko, and C. Daraio, in *Schock Compression of Condensed Matter, 2005*, AIP Conf. Proc. No. 845 (AIP, New York, 2006), pp. 1523–1526; see also e-print arXiv:cond-mat/0512367.
[15] E. B. Herbold and V. F. Nesterenko, Phys. Rev. E **75**, 021304 (2007).
[16] L. D. Landau and E. M. Lifshitz, *Theory of Elasticity* (Addison-Wesley, Massachusetts, 1959), pp. 30.
[17] H. Hertz, J. Reine Angew. Math. **92**, 156 (1881).
[18] A. Rosas and K. Lindenberg, Phys. Rev. E **69**, 037601 (2004).
[19] R. C. Tolman, *The Principles of Statistical Mechanics* (Oxford University Press, London, 1938).